Ecological Indicators 183 (2026) 114670

Contents lists available at ScienceDirect

Ecological Indicators

journal homepage: www.elsevier.com/locate/ecolind

Climate-adjusted time-series analysis of vegetation dynamics following pipeline disturbance and restoration: A proof-of-concept framework

Bojana Petrovic [a,b,*], Mattia Balestra [a,c], Tomáš Mikita [d], Stefano Chiappini [a], Roberto Pierdicca [a]

[a] Department of Construction, Civil Engineering and Architecture (DICEA), Università Politecnica delle Marche, 60131 Ancona, Italy
[b] Department of Geology and Soil Science, Faculty of Forestry and Wood Technology, Mendel University in Brno, Czech Republic
[c] Department of Agricultural, Food and Environmental Sciences (D3A), Università Politecnica delle Marche, 60131 Ancona, Italy
[d] Department of Forest Management and Applied Geoinformatics, Faculty of Forestry and Wood Technology, Mendel University in Brno, Czech Republic

ARTICLE INFO

Keywords:
Sentinel-2
Vegetation indices
Interrupted time-series
Pipeline disturbance
ERA5-land
Vegetation recovery
Climate adjustment

ABSTRACT

Pipeline infrastructure causes abrupt vegetation disturbance, yet restoration effectiveness remains poorly quantified because climate variability and lagged vegetation responses confound observational studies. This proof-of-concept study developed a climate-adjusted interrupted time-series (ITS) framework to evaluate vegetation dynamics following pipeline clearing (November 2020) and replanting (March 2023). The analysis used 65 monthly observations per polygon (3 polygons, 0.42 ha; 195 polygon-month observations) at a study site in Italy. Monthly Sentinel-2 vegetation indices (NDVI, NDRE) and ERA5-Land climate variables (January 2020–May 2025) were analyzed using interrupted time-series models with fixed breakpoints, Fourier seasonality, standardized climate covariates, and polygon fixed effects. UAV multispectral surveys (May 2025, 2 cm resolution) and field measurements validated that fine-scale vegetation establishment was occurring below Sentinel-2's 10 m detection threshold. The framework successfully detected large disturbances: pipeline clearing caused immediate vegetation loss (NDVI -0.536, NDRE −0.368; both $p < 0.001$) followed by significant natural recovery during 2021–2022 (NDVI +0.074 yr^{-1}, NDRE +0.049 yr^{-1}; both $p = 0.015$). After accounting for climate and seasonality, replanting showed no statistically significant site-wide effect (NDVI +0.019, 95% CI: −0.064 to +0.103, $p = 0.650$). UAV validation confirmed localized vegetation establishment (NDVI $r = 0.918$, NDRE $r = 0.841$ with field survival), demonstrating that recovery was occurring at sub-pixel scales but remained below Sentinel-2's detection threshold due to spatial averaging. The climate-adjusted ITS framework provides a replicable, transferable approach for disentangling anthropogenic and environmental drivers where traditional control designs are infeasible. While detecting subtle restoration effects requires larger samples, extended monitoring, or higher-resolution imagery, this demonstrates a methodological advance for climate-aware evaluation of small-scale restoration interventions.

1. Introduction

Linear infrastructure development, including pipeline installations, creates persistent disturbances to vegetation that often alter ecosystem structure and function for years or decades (Shi et al., 2014; Xiao et al., 2016). Such projects can cause lasting soil disturbance, vegetation removal, and altered recovery trajectories, particularly in ecologically fragile regions (Xiao et al., 2014). These disturbances remove existing vegetation through clearing and soil disruption, fragmenting habitats and creating conditions that can slow down natural recovery (Brehm and Culman, 2022). While restoration efforts such as replanting are commonly implemented to accelerate the process, their effectiveness remains difficult to quantify without systematic monitoring frameworks that account for both intervention timing and environmental variability (Wortley et al., 2013; Flemming et al., 2023). As linear infrastructure networks continue to expand globally (Raiter et al., 2018; WWF and Center for Large Landscape Conservation, 2025), quantifying their ecological impacts and restoration outcomes has become increasingly urgent. The challenge is especially pronounced for small-scale restoration, where traditional before–after–control–impact (BACI) designs are often infeasible due to difficulties in identifying suitable untreated control areas (Smokorowski and Randall, 2017). Moreover, disentangling anthropogenic disturbance from climate-driven growth or decline requires integrative monitoring frameworks (England et al.,

* Corresponding author at: Department of Construction, Civil Engineering and Architecture (DICEA), Università Politecnica delle Marche, 60131 Ancona, Italy.
E-mail address: b.petrovic@staff.univpm.it (B. Petrovic).

https://doi.org/10.1016/j.ecolind.2026.114670
Received 24 November 2025; Received in revised form 26 January 2026; Accepted 27 January 2026
Available online 14 February 2026
1470-160X/

2021).

Remote sensing, particularly through vegetation indices (VIs), offers a practical way to monitor vegetation recovery over extended timescales and has been widely used to detect disturbances such as wildfires, forest harvesting, and infrastructure development (Monroe et al., 2020; Taddeo et al., 2022; Lasaponara et al., 2022; Balata et al., 2022). Common indices such as the Normalized Difference Vegetation Index (NDVI) and the Normalized Difference Red Edge (NDRE) provide continuous, repeatable measures of canopy cover, chlorophyll content, and photosynthetic vigor (Tucker, 1979; Barnes et al., 2000; Delegido et al., 2011). Although widely used, these indices are affected by saturation at high biomass levels and soil background effects, particularly in disturbed areas (Yan et al., 2025). Related indices, including the Green NDVI (GNDVI; Gitelson et al., 1996), Soil-Adjusted Vegetation Index (SAVI; Huete, 1988), and Normalized Difference Water Index (NDWI; McFeeters, 1996), provide complementary information on canopy greenness, soil-adjusted vegetation signals, and water content.

However, vegetation index (VI) time series are influenced by seasonal phenology and climate variability, including precipitation, temperature, and soil moisture fluctuations, which complicate the detection of discrete disturbance events. Precipitation regulates soil moisture availability, which in turn influences photosynthetic activity and canopy greenness (Al-Kindi et al., 2023; Mehmood et al., 2024). Disentangling these natural drivers from anthropogenic disturbance requires explicit modeling of lagged climate effects and careful selection of analytical frameworks (Kang et al., 2024). In addition, vegetation responses are often delayed, reflecting antecedent moisture conditions accumulated over weeks to months. The strength of these relationships varies with ecosystem type and seasonal context (Vicente-Serrano et al., 2013; Gao et al., 2024). Temperature affects metabolic rates, growing season length, and vegetation water use, while evapotranspiration integrates the combined effects of energy availability, atmospheric demand, and plant regulation (Baldocchi et al., 2010; Cheng et al., 2024). As vegetation integrates both past and present climatic influences, lagged responses are common and should be explicitly considered in analyses. Integrating VI time series with climate data in interrupted time-series (ITS) analyses helps isolate disturbance effects from seasonal and climatic variability, producing more robust estimates of vegetation impact and recovery (Lopez Bernal et al., 2017; Lopez Bernal et al., 2018).

ITS analysis provides a quasi-experimental framework for estimating intervention effects from observational data by comparing temporal trajectories before and after a defined breakpoint (Linden, 2015). Originally developed for policy evaluation and medical research (Wagner et al., 2002; Ramsay et al., 2003), ITS methods have been adapted for environmental applications where randomized experiments are infeasible (Wauchope et al., 2021). In parallel, remote sensing applications for continuous change detection and land cover classification using high temporal resolution satellite time series (Burkholder et al., 2004; Zhu and Woodcock, 2014) have advanced the ability to capture disturbances and recovery trajectories. Critical to ecological applications is the explicit modeling of seasonality and climate covariates, as phenological cycles and inter-annual climate variability can produce temporal patterns that mimic or obscure intervention effects (Burkholder et al., 2004; Asmala et al., 2021; Delaporte et al., 2022).

Despite these advances in time-series and climate-integrated analyses, few studies have quantified the time lag between restoration implementation and detectable vegetation recovery with satellite observations. Quasi-experimental designs such as BACI analyses have successfully isolated restoration effects in semi-arid and grassland ecosystems using spatial controls (Conner et al., 2016; Smokorowski and Randall, 2017). The BACI designs are constrained by the availability of spatially matched control areas with comparable baseline conditions and climate exposure, which are often absent in linear infrastructure contexts. The ITS framework with climate adjustment provides an alternative approach, allowing intervention effects to be isolated through explicit modeling of temporal trends, seasonality, and climatic covariates rather than spatial controls. For pipeline installations, suitable control sites are rarely available because linear projects lack designated reference areas, and parallel corridors with comparable pre-disturbance vegetation and climate exposure are difficult to identify once disturbance has occurred (Smokorowski and Randall, 2017; Xiao et al., 2014). Other quasi-experimental approaches, such as difference-in-differences or synthetic control methods, similarly depend on appropriate comparison units that are often unavailable for localized infrastructure restoration (Angrist and Pischke, 2009; Abadie et al., 2010; Wauchope et al., 2021). Climate-adjusted interrupted time-series analysis addresses this constraint by using the pre-disturbance period within the same site as the counterfactual baseline (Linden, 2015; Lopez Bernal et al., 2017). In this framework, confounding influences are controlled through explicit modeling of seasonality and climatic variability rather than spatial matching (Delaporte et al., 2022). Fusion of ground-based and satellite observations, with explicit control for phenology and climate variability, offers a robust framework for assessing restoration outcomes and detecting the onset of intervention effects (Meroni et al., 2017; Dronova and Taddeo, 2022; Del Río-Mena et al., 2023). However, previous research has primarily focused on large-scale or natural disturbances such as wildfires and deforestation (Kennedy et al., 2010; Zhao et al., 2018; Zhu et al., 2020), leaving uncertainty about how small-scale infrastructure disturbances recover under active restoration.

This study addresses these gaps through a proof-of-concept application with two objectives: (1) develop a climate-adjusted ITS framework that controls phenology and climatic drivers in vegetation monitoring, and (2) quantify the magnitude and timing of vegetation responses to pipeline disturbance (clearing) and subsequent restoration (replanting). The framework disentangles anthropogenic and environmental drivers of vegetation change in contexts where traditional spatially replicated control-impact designs are logistically infeasible. The single-site proof-of-concept validates the methodology and provides a foundation for multi-site applications across linear infrastructure restoration.

2. Material and methods

2.1. Study area

The monitoring activities took place in a reforestation area at Ponte Baffoni (municipality of Novafeltria, Province of Rimini, Italy; 43.87° N, 12.28° E) (Fig. 1). The site lies in hilly terrain typical of the central Apennines. Within this area, three representative polygons (P1 = 972.86 m^2, P2 = 1735.64 m^2, P3 = 1507.06 m^2, total = 4216 m^2 = 0.4216 ha) were selected for detailed time-series analysis to track vegetation recovery following pipeline installation/clearing in November 2020 and subsequent replanting in March 2023. The polygons were distributed along the pipeline corridor in collaboration with the pipeline operator's environmental monitoring team and correspond to the same compartments that are usually inspected during standard ground-based post-restoration surveys (Fig. 2A). Satellite imagery provides a clear visual record of vegetation change from pre-disturbance conditions through recovery phases (Fig. 2B–D). The region experiences a Mediterranean sub-humid climate (Köppen-Geiger classification Csa) characterized by warm dry summers and cool wet winters (Peel et al., 2007; Beck et al., 2018). Mean annual temperature in the area ranges from approximately 13–14 °C, with July as the warmest month and January as the coldest. Mean annual precipitation is about 850–1000 mm, concentrated between October and April (based on ERA5-Land reanalysis for the study period 2020–2025; Muñoz-Sabater et al., 2021). These seasonal precipitation patterns strongly influence soil moisture availability and vegetation phenology, with peak greenness typically occurring in late spring to early summer.

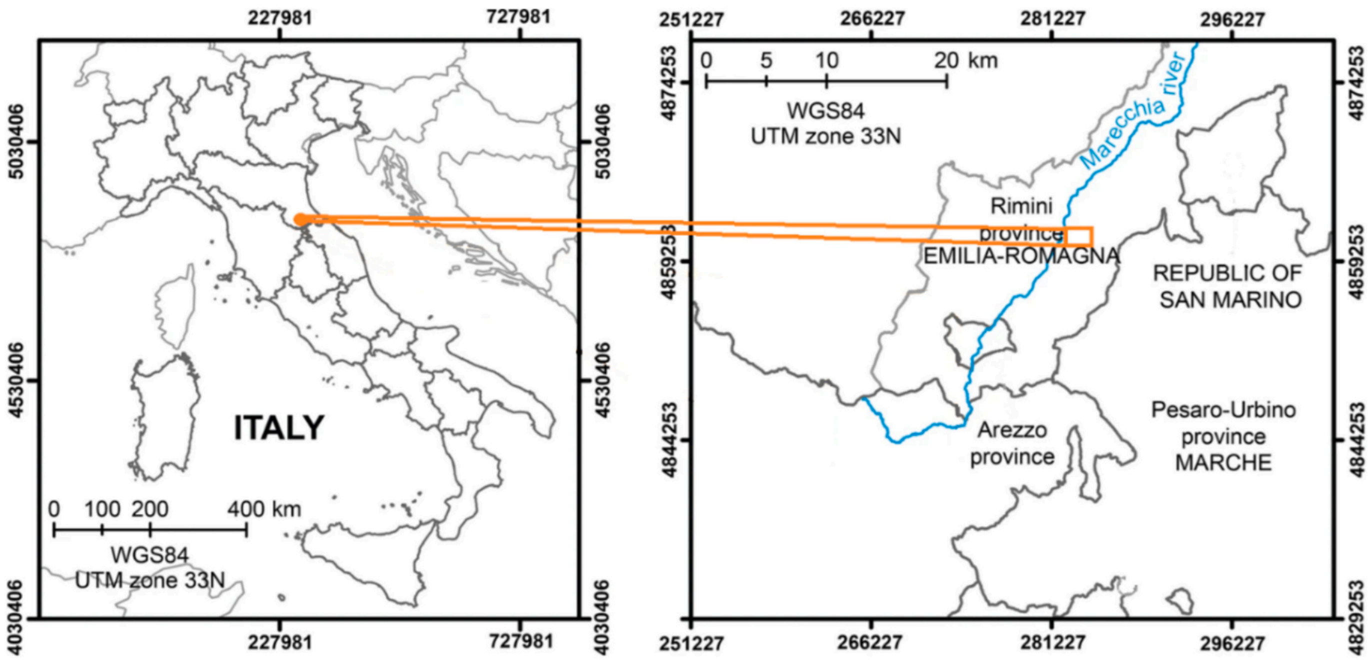

Fig. 1. Geographic location of the study area.

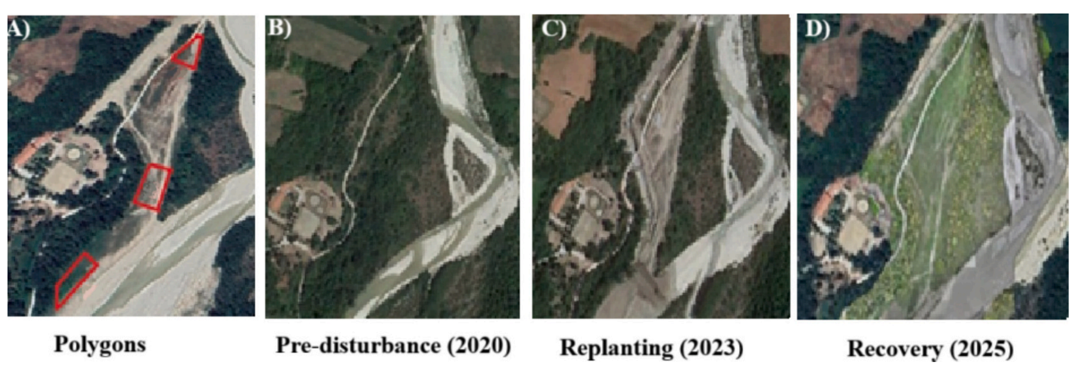

Fig. 2. Visual sequence of polygons, disturbance and recovery at Ponte Baffoni (2020–2025). *Imagery source: Google Earth Pro; © Google 2025, Maxar Technologies.

2.2. Study design

At this site, BACI designs were not feasible due to the absence of suitable control areas with comparable pre-disturbance vegetation structure and climate exposure. Therefore, the study utilized a polygon-month panel design from January 2020 to May 2025, focusing on three fixed polygons (P1-P3) subject to the two interventions described above. This approach allowed for an interrupted time-series analysis to estimate immediate changes in VI levels and subsequent trend shifts after each intervention, while controlling for seasonality and monthly climate variability. The primary VIs analyzed were NDVI and NDRE because they provide complementary information on vegetation structure and physiology. NDVI (near-infrared-red ratio) is strongly correlated with leaf area index and chlorophyll content, making it effective for tracking canopy development (Tucker, 1979; Gitelson et al., 2003). NDRE (near-infrared-red edge ratio) utilizes the red edge band (~705 nm), which is more sensitive to chlorophyll concentration at moderate-to-high leaf area index (LAI) and less prone to saturation under dense canopy conditions (Delegido et al., 2011; Delloye et al., 2018). Together, these indices enable detection of both sparse early regrowth and later-stage canopy recovery. This analytical framework integrated various data sources, including Sentinel-2 satellite imagery, ERA5-Land climate reanalysis, UAV multispectral data, and ground measurements (Fig. 3).

The panel design yielded 195 polygon-month observations (65 months × 3 polygons) for primary interrupted time-series models. The 0–3-month lag window was selected based on evidence that vegetation responses to moisture availability typically manifest within 1–3 months in Mediterranean ecosystems (Vicente-Serrano et al., 2018; Walther et al., 2019), with lag-0 representing immediate effects and longer lags capturing cumulative antecedent conditions. In distributed-lag climate analyses requiring 0–3-month lagged variables, the first three months of each polygon's time series (January–March 2020) were excluded due to insufficient historical data for constructing lag-3 terms, resulting in 186 usable observations (62 months × 3 polygons).

2.3. Data collection, processing and harmonization

Sentinel-2 Level-2 A surface reflectance data (COPERNICUS/S2_SR_HARMONIZED; 10–20 m; MSI) were accessed via Google Earth Engine (GEE) (Gorelick et al., 2017; Drusch et al., 2012) for January 2020–May 2025. Sentinel-2 imagery has proven effective for forest disturbance monitoring (Pałaś and Zawadzki, 2020), providing suitable spectral and temporal resolution for detecting anthropogenic impacts. With global availability beginning in 2017, Sentinel-2 provides a 5-day

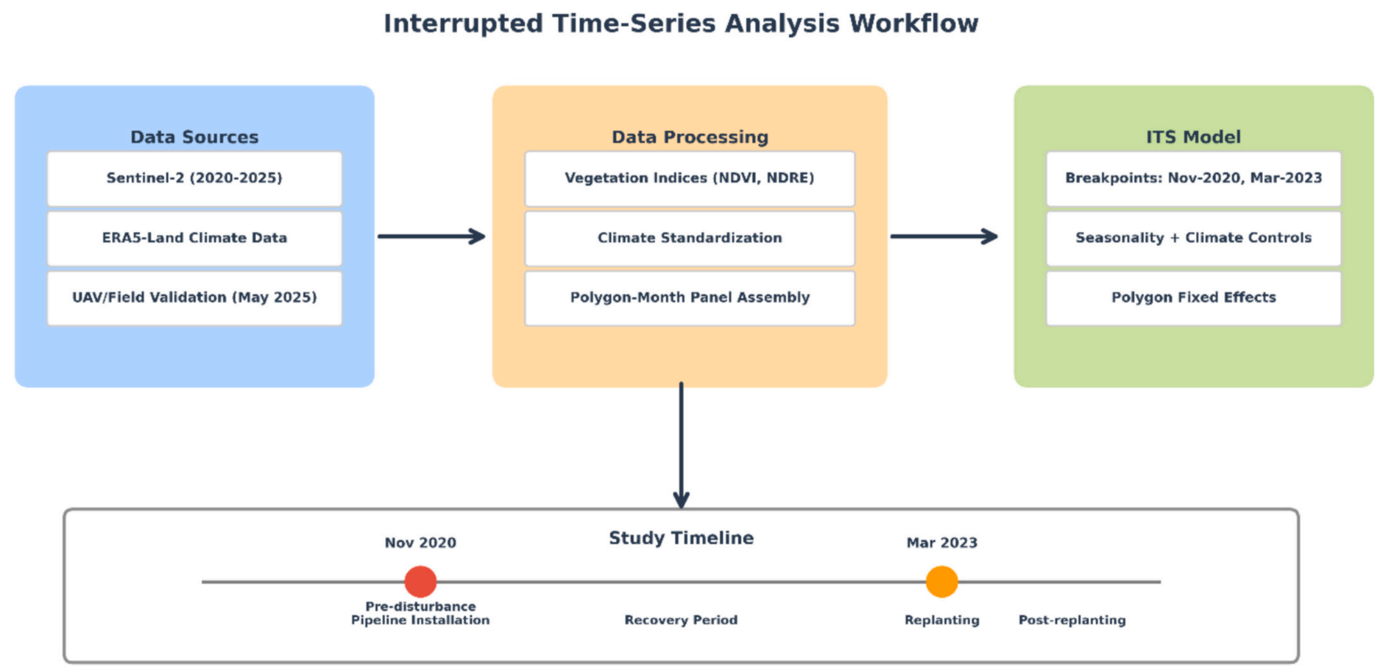

Fig. 3. Study workflow.

revisit period and 10 m spatial resolution, offering sufficient temporal and spatial coverage for monitoring vegetation changes and evaluating recovery. For each calendar month, the single Sentinel-2 scene with the lowest cloud cover percentage (CLOUDY_PIXEL_PERCENTAGE) over the study area was selected. This single-scene approach was adopted to preserve temporal precision for ITS analysis, avoiding temporal averaging artifacts that could obscure abrupt changes at the monthly breakpoints. Vegetation indices (NDVI, NDRE, GNDVI, SAVI, NDWI) were computed from each monthly scene using band arithmetic, and polygon-mean values were extracted at 10 m resolution using reduceRegions function (scale: 10, tileScale: 4) in GEE (Table 1). For indices requiring 20 m resolution bands (e.g., NDRE via B5), GEE's default bilinear resampling upsampled B5 to 10 m so that all band arithmetic operated on a common 10 m grid. The monthly series represent polygon-level spatial averages rather than per-pixel or per-tree measurements.

Monthly climate variables were obtained from ERA5-Land reanalysis (Muñoz-Sabater et al., 2021; Copernicus Climate Change Service, 2019) via GEE for the same period. Variables included 2-m air temperature, total precipitation, evapotranspiration, and top-layer soil moisture (0–7 cm). These variables were selected to represent key climatic drivers of vegetation greenness: temperature controls metabolic rates and growing season length; precipitation provides water inputs; evapotranspiration represents atmospheric demand; and top-layer soil moisture (0–7 cm) directly reflects plant-available water in the root zone. A water-deficit index (precipitation minus evapotranspiration) was derived to capture the balance between water supply and demand, and a lag-1 soil-moisture series was created. Daily ERA5-Land fields were aggregated to monthly values: temperature as monthly means (converted from Kelvin to °C); precipitation and evapotranspiration as monthly sums (converted from meters to millimeters by ×1000, with evapotranspiration converted to positive values representing water loss); soil moisture as monthly means. Since ERA5-Land has a native resolution of ~0.1° (~9–11 km), climate conditions were treated as site-level with the same monthly values assigned to all polygons.

To validate whether fine-scale vegetation recovery was occurring below Sentinel-2's detection threshold, UAV multispectral surveys and field measurements were conducted at the end of the monitoring period (May 2025). This timing coincided with peak vegetation period in the Mediterranean climate, when canopy development is complete and chlorophyll activity is at maximum, providing optimal conditions for vegetation index assessment. This single-date survey captured VI-field relationships at peak growing conditions. Seasonal variation in these correlations (e.g., during winter dormancy) was not assessed but would provide insight into temporal stability across phenological stages. UAV surveys used a MicaSense Altum-PT multispectral sensor mounted on a DJI Matrice 350 RTK platform. Flight missions were planned using DJI Fly 2 and executed at 45 m above ground level with a cruising speed of 4 m/s, achieving 80% forward and 70% side overlap and yielding a ground sampling distance (GSD) of 2 cm/pixel-approximately 500× finer pixel size than Sentinel-2's 10 m pixels. The sensor captured five spectral bands (Blue, Green, Red, Red Edge, Near-Infrared; 475–840 nm), with radiometric calibration performed using certified reflectance targets and georeferencing via ground control points (GCPs) to ensure positional accuracy. Vegetation indices (NDVI, NDRE, GNDVI, SAVI, NDWI) were computed using the same band-ratio formulas as Sentinel-2 (Table 1), adapted to the Altum-PT spectral configuration. Polygon-level VI values were extracted as spatial means across all 2 cm pixels within each polygon boundary using zonal statistics in ArcGIS Pro, providing single representative values per polygon directly comparable to Sentinel-2's polygon-averaged observations. The validation framework quantified whether UAV-derived VIs could detect fine-scale establishment patterns not resolvable at Sentinel-2's 10 m resolution by computing Pearson correlation coefficients between UAV VI values and field-measured tree survival rates (n = 3 polygons), with scatter plots provided in Supplementary Figs. S4 and S5. Ground-based observations collected concurrently included tree survival rate (%), mean height (m), and mean stem diameter (cm) for each polygon.

This validation assessed two aspects of restoration effectiveness: (1) the relationship between remotely sensed vegetation indices and field-

Table 1
Selected spectral indices and their equations using Sentinel-2 bands.

Index	Index formula	Reference
NDVI	(B8 − B4) / (B8 + B4)	Tucker, 1979
NDRE	(B8 − B5) / (B8 + B5)	Barnes et al., 2000
GNDVI	(B8 − B3) / (B8 + B3)	Gitelson et al., 1996
SAVI	(1 + L)(B8 − B4) / (B8 + B4 + L) with L = 0.5	Huete, 1988
NDWI	(B3 − B8) / (B3 + B8)	McFeeters, 1996

measured vegetation establishment (survival, growth), and (2) the spatial heterogeneity of recovery at fine scales (2 cm) that would be averaged within Sentinel-2's 10 m pixels. These single-date observations were not incorporated into the interrupted time-series model parameter estimation.

2.4. Methodology

2.4.1. ITS specification and estimation

Level and post-breakpoint trend changes were estimated using segmented (interrupted) time-series regression with seasonality (sin/cos) and climate covariates. Breakpoints were fixed a priori at November 2020 (pipeline installation and clearing) and March 2023 (replanting). Following Lopez Bernal et al. (2017), we specified an interrupted time-series model with Fourier seasonality terms and climate covariates, for outcome VI_{it}, the model specification was:

$$VI_{it} = \alpha + \phi_1 \sin\left(\frac{2\pi m_t}{12}\right) + \phi^2 \cos\left(\frac{2\pi m_t}{12}\right)$$

$$+ \beta_1 post2020_t + \beta_2 time\_since\_2020_t$$

$$+ \beta_3 post2023_t + \beta_4 time\_since\_2023_t$$

$$+ \gamma_1 Temp_t^{(sc)} + \gamma_2 Deficit_t^{(sc)} + \gamma_3 SoilM_{t-1}^{(sc)}$$

$$+ \delta_i + \varepsilon_{it} \tag{1}$$

where: VI_{it} = vegetation index (NDVI or NDRE) for polygon $_i$ at time $_t$. α = overall intercept (baseline vegetation index level)Seasonality = $\phi_1 \sin(2\pi m_t/12) + \phi_2 \cos(2\pi m_t/12)$, where: ϕ_1, ϕ_2 = seasonality coefficients m_t = month index (1−12) in the sin/cos terms

Higher-order Fourier harmonics were explored during model development. They were not retained because they provided negligible improvement in model fit while increasing parameter complexity relative to the limited spatial sample.

Intervention terms:

β_1 = level change coefficient at November 2020 breakpoint

β_2 = slope change coefficient after November 2020

β_3 = level change coefficient at March 2023 breakpoint

β_4 = slope change coefficient after March 2023

$post2020_t$, $post2023_t$ = post-intervention indicators (0 before, 1 after breakpoint)

$time\_since2020_t$, $time\_since2023_t$ = time since each breakpoint (in years). Time was indexed in monthly steps and rescaled to years for interpretability of slope coefficients

Climate covariates (sc = standardized/z-scored):

γ_1, γ_2, γ_3 = climate effect coefficients

$Temp_t(sc)$ = standardized temperature

$Deficit_t(sc)$ = standardized water deficit (precipitation-evapotranspiration)

$SoilM_{t-1}(sc)$ = standardized lagged soil moisture (1-month lag)

$\boldsymbol{\delta_i}$ = polygon fixed effects (polygon-specific intercepts controlling for time-invariant differences among the three polygons)

ε_{it} = error term

A lag sensitivity analysis was conducted for soil moisture at 0–3-month lags to evaluate delayed vegetation responses. Distributed-lag ITS models were used to compare alternative lag structures and climate drivers based on changes in model fit (Partial R^2 and AIC; Supplementary Table S4). Based on these criteria, a one-month lagged soil moisture term ($SoilM_{t-1}$) was selected for the primary ITS specification, as it captures short-term antecedent water availability while maintaining model parsimony. Longer lag structures were not retained because they did not provide sufficient improvement in fit relative to the increase in parameter complexity given the limited spatial sample. Potential multicollinearity among climate variables was addressed through this model selection approach. Soil moisture was chosen over other climate drivers (precipitation, evapotranspiration, water deficit) based on superior model fit as assessed by Partial R^2 and AIC (Supplementary Table S4). Testing climate drivers separately rather than simultaneously minimizes multicollinearity concerns. Overall R^2 is reported for the full ITS model, along with the partial R^2 for the intervention block. Partial R^2 quantifies the increase in explained variance obtained by adding the four intervention terms (post2020, time_since_2020, post2023, time_since_2023) to a baseline model that already includes seasonality, climate covariates, and polygon fixed effects. In this way, partial R^2 quantifies the unique contribution of the interventions beyond climate, seasonality, and polygon effects. Standard errors were clustered by month to account for shared climate conditions across polygons within each time period. 95% confidence intervals (CIs) were reported for all regression coefficients as direct measures of estimation precision and to indicate the range of effect sizes consistent with the data. Under this specification, β_1 and β_2 quantify the immediate impact and recovery trend following pipeline clearing. β_3 and β_4 represent the immediate level change and subsequent trend following replanting. These terms implicitly assume that intervention effects are detectable at the satellite observation scale.

2.4.2. Counterfactual predictions

To visualize the impact of the interventions by polygon, model-based counterfactual trajectories were generated from the pooled ITS fit. Predictions were computed twice for each polygon-month: (i) the fitted trajectory using the estimated model as specified (seasonality, standardized climate covariates, polygon fixed effects, and the four intervention terms), and (ii) a no-intervention counterfactual obtained by setting the intervention variables to zero (post2020 = time_since_2020 = post2023 = time_since_2023 = 0) while keeping month, climate, and polygon effects exactly as observed. Counterfactuals are descriptive outputs from the same fitted model (no re-fitting); inference in the paper relies on the ITS coefficients with month-clustered standard errors.

2.4.3. Climate-vegetation index sensitivity

Drivers of month-to-month variability were evaluated using lags 0–3 months of precipitation, evapotranspiration, water deficit (precipitation-evapotranspiration), and soil moisture. Lag-3 variables require three prior months of climate data for each vegetation observation. Consequently, the first three months of the time series (January–March 2020) were excluded from the distributed-lag analysis, as these months lacked sufficient historical climate data (October–December 2019). Analyses used the 186 polygon-month observations (excluding the first three months for lag-3 construction, as described in Study Design). Firstly, descriptive Pearson correlations were computed at lags 0–3 on polygon-level monthly means (heatmaps). Secondly, each driver's 0–3-month lag block was added in separate models to the baseline ITS (seasonality + intervention terms + polygon fixed effects), and partial R^2 for the lag block and ΔAIC (full-baseline) were calculated; standard errors were clustered by month to account for shared site-level climate shocks.

2.4.4. Seasonal anomalies

Monthly anomalies were obtained by subtracting the polygon-specific month-of-year mean (2020–2025) from each polygon-month value (i.e., VI minus seasonal climatology). Anomalies were summarized for three periods: Pre-clearing 2020 (Jan-Oct 2020), Post-clearing (November 2020–December 2022), and Post-replant (March 2023–May 2025). Between-period differences are reported as mean contrasts with bootstrap 95% CIs.

2.4.5. Sensitivity analyses and software

Sensitivity analyses repeated the same ITS specification for GNDVI, SAVI, and NDWI using the same model structure as the primary analyses (seasonality via sin/cos, standardized climate covariates, polygon fixed effects, month-clustered SEs, breakpoints at November 2020 and March

2023). *Per*-polygon heterogeneity was explored in a supplementary analysis by interacting intervention terms with polygon. Residual diagnostics were inspected and showed patterns comparable to NDVI/NDRE. Accordingly, for these indices, coefficients and model fit are reported in Supplementary Tables S1 and S2 and include observed-fitted plots (Supplementary Figs. S1, S2 and S3).

2.4.6. Statistical power and detectability analysis

Given the proof-of-concept design with $n = 3$ polygons, we conducted a model-based detectability analysis to quantify the minimum detectable effect size (MDES) for intervention effects. The MDES calculation follows standard power analysis conventions (Cohen, 1988; Bloom, 1995), using $\alpha = 0.05$ (two-tailed) and 80% power as conventional thresholds for adequately powered studies. The MDES represents the smallest effect that could be detected with these criteria, calculated as:

$$MDES = \left(z\_\{\alpha/2\} + z\_\{\beta\}\right) \times SE \tag{2}$$

where z_{α/2} = 1.96 (critical value for two-tailed α = 0.05), z_{β} = 0.84 (critical value for 80% power), and SE is the cluster-robust standard error of the intervention coefficient from the ITS model (Eq. (1)). This calculation quantifies the design's capability to detect effects of varying magnitudes. All analyses were performed in Python (Jupyter), using pandas for data wrangling, statsmodels for OLS with cluster-robust SEs, and matplotlib for figures. Satellite preprocessing was carried out in Google Earth Engine; ERA5-Land data were aggregated to monthly values before merge.

3. Results

3.1. Effects of pipeline installation (2020) and replanting (2023)

Interrupted time-series models detected a large, immediate decline in vegetation following the November 2020 pipeline installation for both indices (Table 2; *per*-polygon results in Supplementary Table S3). NDVI decreased by 0.536 (95% CI −0.630, −0.443; $p < 0.001$) and NDRE by 0.368 (95% CI −0.437, −0.298; $p < 0.001$). After this breakpoint, both indices exhibited significant positive recovery trends during 2021–2022: NDVI slope + 0.074 yr^{-1} (95% CI +0.014, +0.134; $p =$ 0.015) and NDRE slope + 0.049 yr^{-1} (95% CI +0.009, +0.088; $p =$ 0.015).

In models that controlled for climate and seasonality, replanting (March 2023) showed no statistically significant effect on either index (NDVI: $\beta_3 = +0.019$, 95% CI: −0.064 to +0.103, $p = 0.650$; NDRE: $\beta_3 =$ +0.004, 95% CI: −0.051 to +0.060, $p = 0.874$). The wide confidence intervals and non-significant *p*-values indicate that the replanting effect, if present, was not detectable at the Sentinel-2 spatial resolution (10 m) and sample size ($n = 3$ polygons) used in this analysis. However, multiscale validation using high-resolution UAV observations (Part 3.6 below) demonstrated that localized vegetation establishment was occurring (NDVI $r = 0.918$, NDRE $r = 0.841$) confirming that the non-significant result across both vegetation indices reflects spatial scale constraints rather than absence of vegetation response.

Table 2
Key intervention effects (NDVI & NDRE).*

VI	Effect	Estimate	95% CI	*p*-value
NDVI	Level change at Nov 2020	-0.536	−0.630, −0.443	<0.001
NDVI	Slope after 2020	+0.074	+0.014, +0.134	0.015
NDVI	Level change at Mar 2023	+0.019	−0.064, +0.103	0.650
NDVI	Slope after 2023	−0.022	−0.087, +0.044	0.512
NDRE	Level change at Nov 2020	−0.368	−0.437, −0.298	<0.001
NDRE	Slope after 2020	+0.049	+0.009, +0.088	0.015
NDRE	Level change at Mar 2023	+0.004	−0.051, +0.060	0.874
NDRE	Slope after 2023	−0.018	−0.061, +0.025	0.401

* Note: Cluster-robust standard errors by month; slopes are per year; 95% confidence intervals.

3.2. Per-polygon counterfactuals

Per-polygon trajectories compared with modelled no-intervention counterfactuals illustrate the magnitude and persistence of the 2020 disturbance (Fig. 4A and B). For both indices, all polygons show a sharp drop immediately after November 2020, with observed values well below the counterfactual during 2021–2022. The gap narrows through 2024–2025, indicating recovery, and there is no clear additional step at March 2023 once seasonality and climate are held constant, consistent with the pooled ITS estimates (Table 2; per-polygon Supplementary Table S3). Although differences among polygons are modest overall, post-2023 slopes are not identical for NDVI: P1 is slightly negative while P2 and P3 are near zero to slightly positive, indicating mild heterogeneity in recovery trajectories.

3.3. Sensitivity analyses

Sensitivity analyses using alternative vegetation indices GNDVI, SAVI, and NDWI confirmed the main disturbance and recovery patterns observed with NDVI and NDRE, though effect magnitudes and directions varied by index (Supplementary Table S1). GNDVI showed a moderate negative disturbance (−0.411, 95% CI -0.490, −0.331; $p < 0.001$) with non-significant post-2020 recovery slope (+0.045 yr^{-1}, $p = 0.105$), suggesting less pronounced recovery signal in the green-NIR domain. SAVI exhibited the largest disturbance magnitude (−0.804, 95% CI-0.944, −0.664; $p < 0.001$) followed by significant recovery (+0.110 yr^{-1}, 95% CI +0.021, +0.200; $p = 0.015$), reflecting its enhanced sensitivity to bare-soil exposure. NDWI displayed an inverted response, with a positive level change in November 2020 (+0.411, 95% CI +0.331, +0.490; $p < 0.001$), consistent with exposed soil moisture following canopy removal. As with NDVI and NDRE, none of the alternative indices detected a significant level or slope change following the March 2023 replanting (all $p > 0.24$). Observed vs fitted trajectories for GNDVI, SAVI, and NDWI are presented in Supplementary Figs. S1–S3, showing model fits comparable to NDVI and NDRE (overall $R^2 =$ 0.72–0.75; Supplementary Table S2).

3.4. Model fit and variance

The intervention terms (level and slope changes at both breakpoints) explained a large share of variation beyond climate, seasonality, and polygon effects: Partial $R^2 = 0.675$ for NDVI and 0.659 for NDRE (Table 3). Overall model fit was high ($R^2 = 0.753$ for NDVI; 0.743 for NDRE), indicating that the ITS models captured the main temporal signals.

The observed and fitted mean trajectories (Figs. 5–6) show no clear additional level shift at March 2023. Fitted lines closely track the observations, consistent with the high overall R^2 values reported in Table 3 (NDVI 0.753; NDRE 0.743). These patterns align with the formal interrupted time-series estimates in Table 2. The models indicate a large negative level shift at the 2020 breakpoint for both NDVI and NDRE, followed by significant positive recovery slopes through 2021–2022, with no statistically significant additional level or slope change at the 2023 breakpoint after adjusting for climate and seasonality.

3.5. Climate-vegetation index sensitivity

Pearson correlations between climate variables and vegetation indices showed varied patterns across lag intervals (Fig. 7A and B). Both indices co-varied positively with evapotranspiration at 1–2-month lags (NDVI $r \approx 0.33$–0.37; NDRE $r \approx 0.38$–0.40), while precipitation showed weaker, short-lived positive associations ($r \approx 0.16$–0.21 at lag 0–1). Soil moisture exhibited modest negative correlations (≈ -0.13 to −0.19),

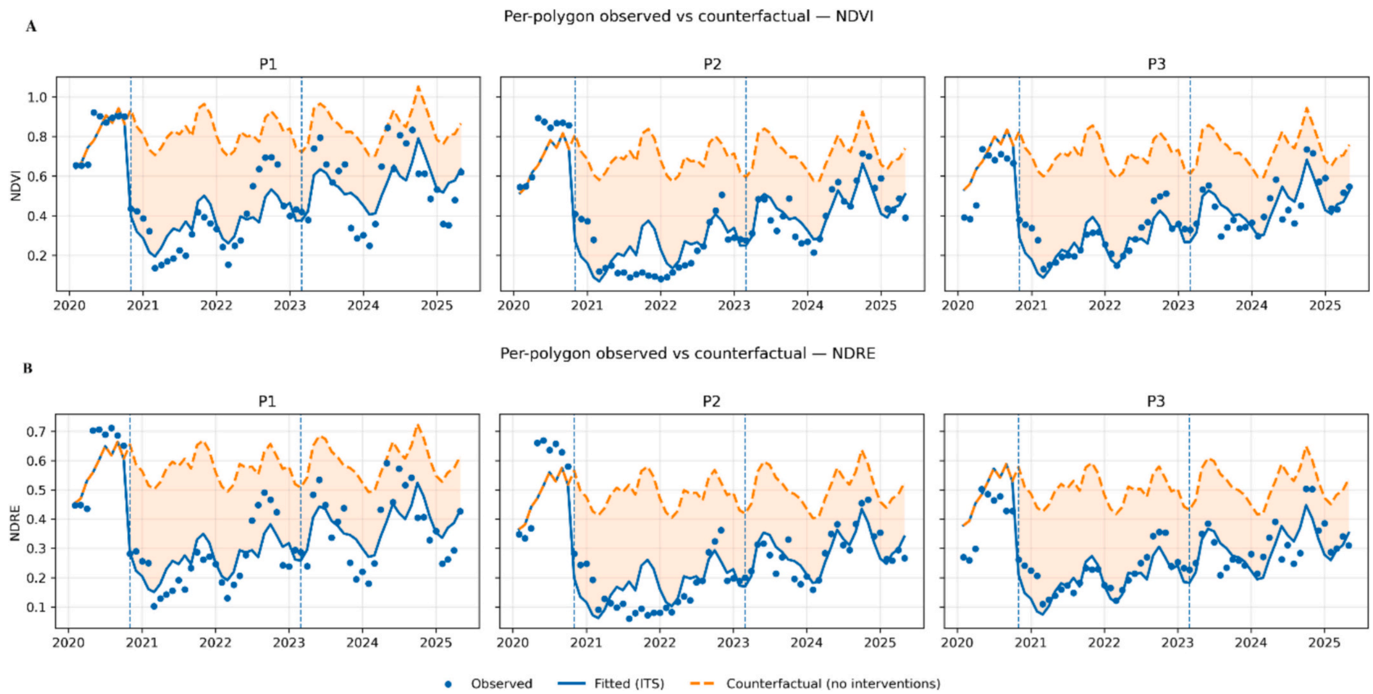

Fig. 4. Per-polygon observed vs counterfactual trajectories (A) NDVI (B) NDRE. Blue dots: observed monthly values; blue line: fitted ITS model; orange dashed line: counterfactual (no interventions). Vertical dashed lines mark intervention dates (November 2020 clearing, March 2023 replanting). Shaded area represents difference between observed and counterfactual trajectories. (For interpretation of the references to colour in this figure legend, the reader is referred to the web version of this article.)

Table 3
Model fit-Partial R^2 (intervention block) & overall R^2.

VI	Partial R^2	Overall R^2
NDVI	0.675	0.753
NDRE	0.659	0.743

*Partial R^2 quantifies variance explained by intervention terms beyond seasonality, climate covariates, and polygon effects. Overall R^2 is for the full model.

and water deficit became more negative by lag 3 (≈ -0.24 to -0.28). The distributed-lag ITS (Supplementary Table S4) indicated that the soil-moisture lag block (0–3 months) provided the largest unique improvement in model fit once seasonality and the 2020/2023 breakpoints were controlled.

In contrast to the raw negative correlations (as mentioned above, Fig. 7A and B), the distributed-lag ITS after controlling for seasonality and interventions revealed positive coefficients for soil moisture (Fig. 8A and B), showing that soil moisture adds the largest unique explanatory power for monthly VI fluctuations. The per-lag coefficients show positive effects at lag 0–1 that decline toward zero by lag 3, indicating that the raw negative correlations were confounded by seasonality (high moisture in winter when VIs are naturally low). This pattern indicates that vegetation greenness is most strongly influenced by soil moisture from the current month and 1 month prior, with effects declining to negligible levels by 3 months.

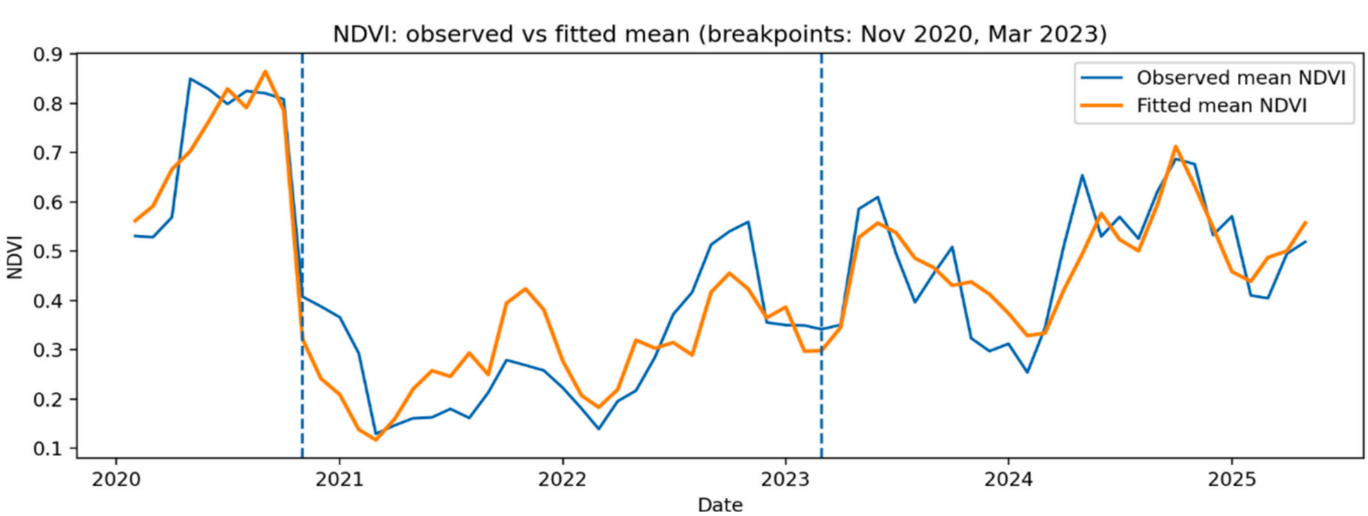

Fig. 5. Observed vs fitted mean NDVI (Jan 2020-May 2025).

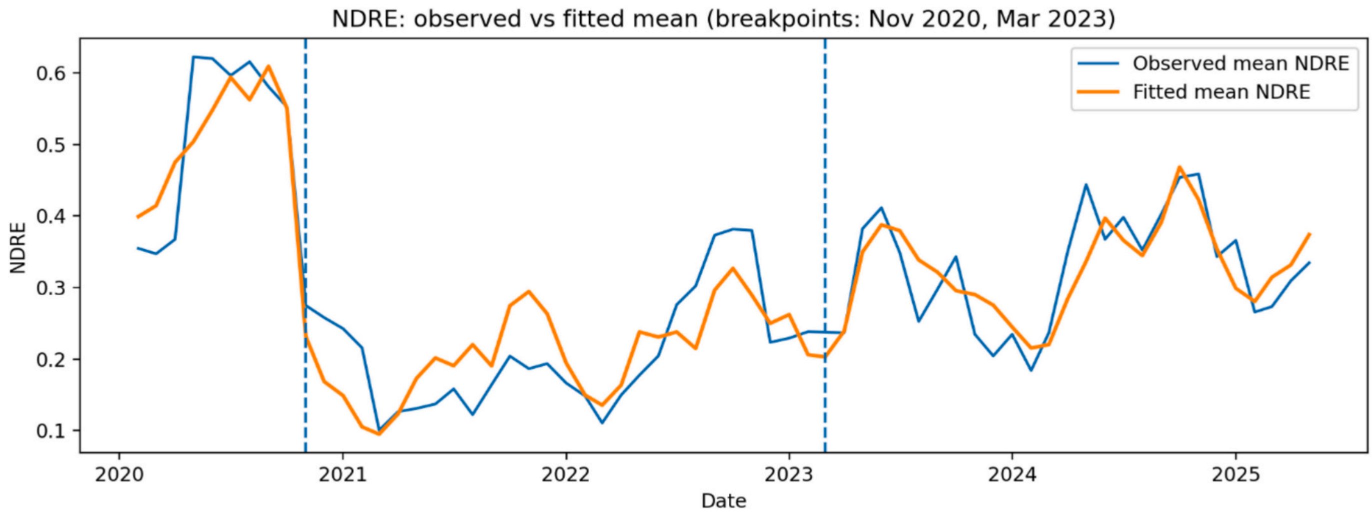

Fig. 6. Observed vs fitted mean NDRE (Jan 2020-May 2025).

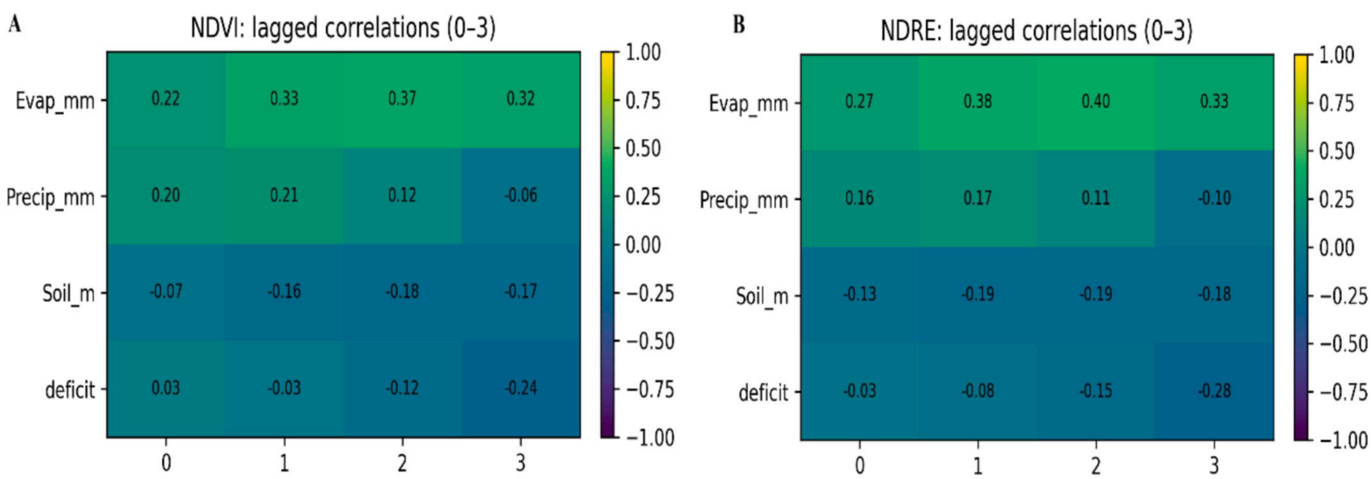

Fig. 7. Lagged climate-vegetation correlations (0–3 months), A-NDVI, B-NDRE. Evap_mm = evapotranspiration; Precip_mm = precipitation; Soil_m = soil moisture; deficit = water deficit.

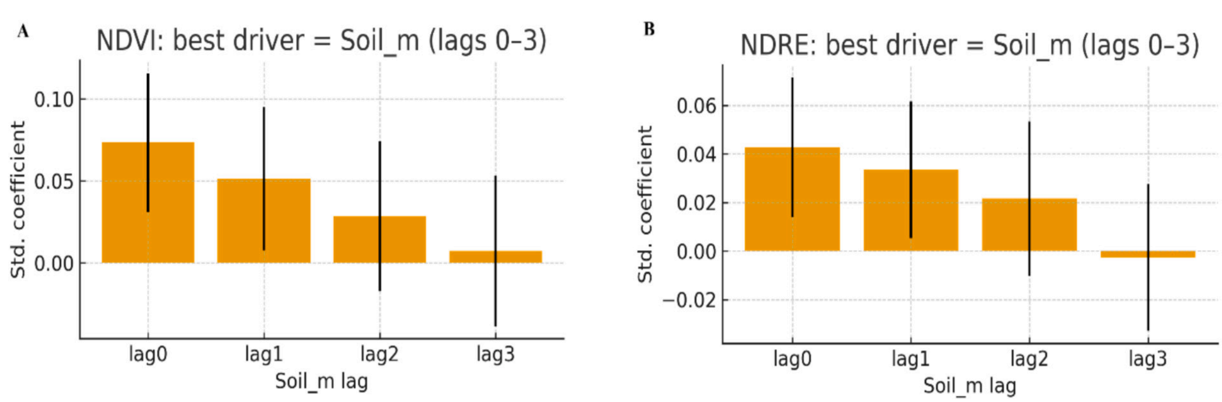

Fig. 8. Distributed-lag ITS coefficients for the best climate driver (soil moisture), standardized coefficients ±95% CI (A-NDVI, B-NDRE).

3.6. *Seasonal anomaly contrasts across intervention periods and UAV-field observations*

Seasonally de-trended anomalies corroborated the ITS findings (Fig. 9). Relative to Pre-clearing 2020, mean anomalies were negative during the Post-clearing period (Nov 2020-Dec 2022) and then moved back toward zero in the Post-replant period (Mar 2023-May 2025). High-resolution UAV validation (May 2025) confirmed localized vegetation establishment below Sentinel-2's detection threshold. UAV vegetation indices showed strong correlations with field-measured tree survival across the three polygons (NDVI: $r = 0.918$; NDRE: $r = 0.841$; Supplementary Table S5, Supplementary Figs. S4 and S5). Tree survival ranged from 29% (Polygon 2) to 70% (Polygon 1), with corresponding variation in UAV-derived indices (NDVI: 0.63–0.73; NDRE: 0.31–0.39). Correlations with mean tree height were negligible (NDVI: $r = -0.112$; NDRE: $r = 0.051$), while correlations with mean stem diameter were strongly negative (NDVI: $r = -0.852$; NDRE: $r = -0.926$). Visual examination of UAV imagery (2 cm GSD) revealed substantial within-polygon spatial heterogeneity, with replanted trees and naturally regenerating vegetation occurring in discrete patches interspersed with bare soil and herbaceous cover. Each polygon contained only 10–17 Sentinel-2 pixels (10 m resolution).

3.7. Model diagnostics

Residual series for both NDVI and NDRE fluctuated around zero with no sustained drift across the November 2020 and March 2023 breakpoints (Fig. 10), indicating no missing trend/seasonality and no evidence that the intervention dates were mis-specified. Together with month-clustered standard errors, these checks support the validity of the ITS estimates.

3.8. Detectability analysis

The minimum detectable effect size (MDES) analysis quantified the study's ability to detect site-wide replanting effects. For the replanting level effect (β_3), the observed cluster-robust standard errors yielded MDES = ±0.119 for NDVI and ± 0.079 for NDRE at 80% power (α = 0.05, two-tailed), corresponding to approximately 22% of the respective clearing effect magnitudes. The observed replanting effects (NDVI +0.019, 95% CI: −0.064 to +0.103; NDRE +0.004, 95% CI: −0.051 to +0.060) were substantially smaller than these detection thresholds. In contrast, the pipeline clearing disturbance (NDVI -0.536, NDRE −0.368) exceeded the MDES by a factor of 4.5–4.6, enabling robust detection (both $p < 0.001$). This confirms that the $n = 3$ polygon design was adequate for detecting large anthropogenic disturbances but underpowered for subtle site-wide restoration effects.

4. Discussion

The observed disturbance magnitude and recovery rates provide quantitative benchmarks for Mediterranean forest ecosystems. The immediate vegetation loss following pipeline installation (NDVI -0.536, NDRE −0.368) aligns with prior reports showing that pipeline construction removes canopy and topsoil, creating linear open areas with abrupt transitions to adjacent forest (Balbuena et al., 2019; Naeth et al., 2020; MacDonald et al., 2020). By explicitly controlling for seasonality and climate variability, these findings demonstrate that pipeline construction produces statistically robust and persistent reductions in canopy greenness requiring multi-year recovery. The recovery rates observed during 2021–2022 (NDVI +0.074 yr^{-1}, NDRE +0.049 yr^{-1}) were slower than those following natural disturbances such as wildfire or harvest (Pickell et al., 2016; White et al., 2017) but comparable to other linear infrastructure projects (Filicetti and Nielsen, 2020). These moderate rates likely reflect soil compaction, altered drainage, and limited seed dispersal that constrain regrowth-a pattern consistent with post-disturbance soil structure changes described by Brehm and Culman (2022).

These findings complement pipeline restoration research spanning multiple continents and ecosystems (Table 4). Comparative studies have employed field-based monitoring from single-year chronosequences (Finnegan et al., 2023) to multi-decadal surveys (Filicetti and Nielsen, 2020; Shaughnessy et al., 2021). They span boreal peatlands and forests, temperate mixed forests (Flemming et al., 2023), grasslands (Naeth et al., 2020; Eduardo-Palomino et al., 2025), semi-arid steppes (Bayramov et al., 2016), and native rangelands (Ostermann et al., 2023), incorporating both field surveys and remote sensing approaches (Bayramov et al., 2016; Eduardo-Palomino et al., 2025). While these studies have primarily used empirical monitoring or chronosequence designs, recent methodological advances have introduced AI-based forecasting approaches to vegetation recovery monitoring. Galdelli et al. (2025), studying a gas pipeline in Mediterranean mixed forests in Italy (Rimini-Sansepolcro), integrated multi-sensor satellite data (Sentinel-2, Landsat-8, PlanetScope) with deep learning models (Prophet, NeuralProphet, LSTM, N-BEATS) to predict NDVI recovery trajectories over 90-day horizons. While their approach demonstrated strong predictive performance in controlled scenarios, it did not incorporate climate covariates or account for confounding environmental variability-a critical limitation when distinguishing recovery from seasonal or climatic effects (Vicente-Serrano et al., 2013; Lopez Bernal et al., 2018).

The broadly consistent responses across multiple vegetation indices (NDVI, NDRE, GNDVI, SAVI) provide convergent evidence of disturbance and subsequent recovery, though effect magnitudes differed by index. SAVI showed the largest negative disturbance signal (−0.804), as expected under sparse cover, because SAVI explicitly reduces soil-background effects, accentuating canopy loss when bare soil is exposed (Huete, 1988; Qi et al., 1994). In contrast, NDWI increased after clearing, consistent with greater visibility of moist substrate/open water following canopy removal; NDWI is designed to enhance water signals (green-NIR) and/or canopy liquid water (NIR-SWIR) (McFeeters, 1996; Gao, 1996). The red-edge/green indices (NDRE, GNDVI) were comparatively stable yet responsive, aligning with evidence that these bands are sensitive to chlorophyll and less prone to NDVI-type saturation at low-moderate LAI suited to early regrowth before full canopy closure (Delegido et al., 2011; Delloye et al., 2018).

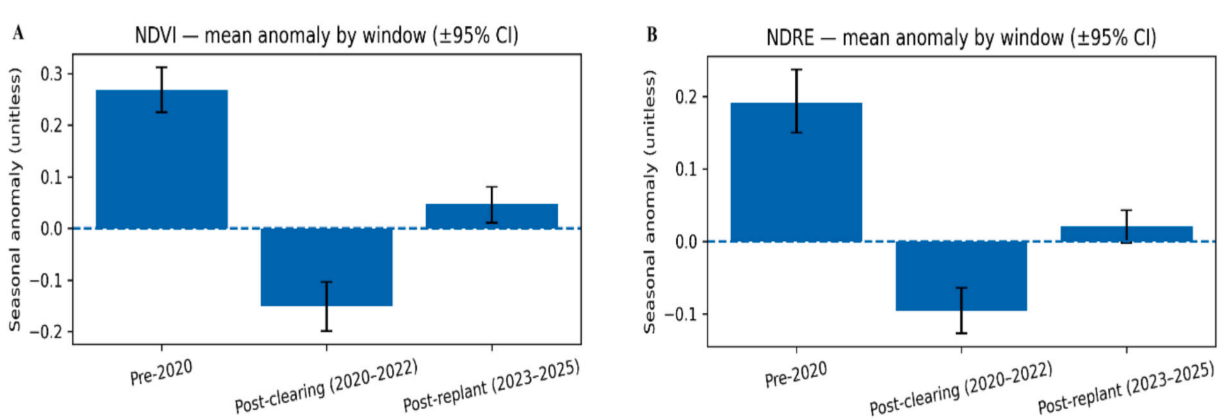

Fig. 9. Mean seasonal anomalies for NDVI (A) and NDRE (B). Bars show polygon-level monthly anomalies (index minus month-of-year mean per polygon) summarized for Pre-clearing 2020 (Jan-Oct 2020), Post-clearing (Nov 2020-Dec 2022), and Post-replant (Mar 2023-May 2025). Error bars are bootstrap 95% Cis.

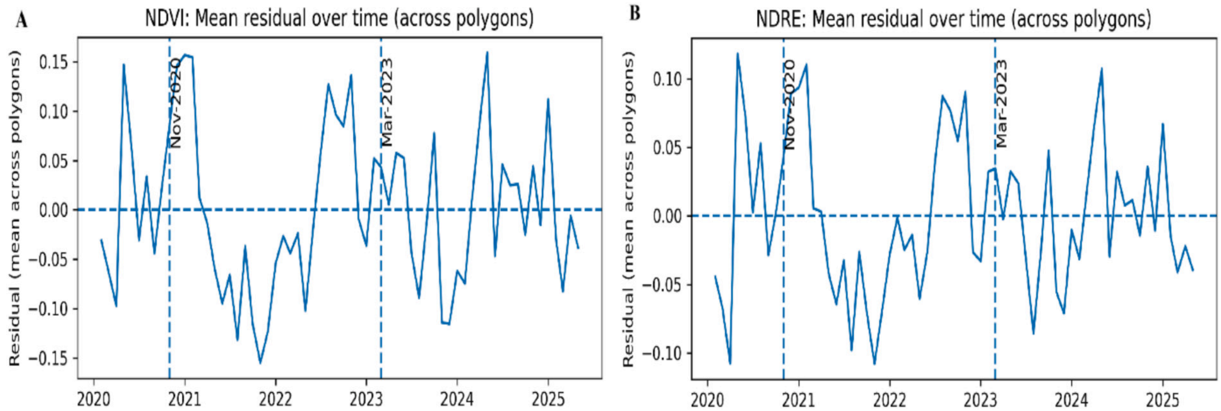

Fig. 10. Residuals over time for NDVI (A) and NDRE (B).

Table 4
Pipeline restoration studies: methodological comparison.

Study	Location	Ecosystem	Monitoring duration	Primary methods	Key approach
This study	Italy	Mixed forest	5.5 years	VIs (remote sensing)	Satellite time-series with climate adjustment
Galdelli et al. (2025)	Italy	Mixed forest	6+ years	Multi-sensor NDVI + AI	Deep learning forecasting (Prophet, LSTM, N-BEATS)
Filicetti and Nielsen (2020)	Canada	Treed peatlands	15+ years	Tree density (field)	Multi-decadal field monitoring
Flemming et al. (2023)	USA	Mixed forest	10 years	Cover, richness, diversity (field)	Chronosequence comparison to reference sites
Naeth et al. (2020)	Canada	Mixed-grass prairie	10 years	Cover, composition (field)	Long-term plot monitoring with treatments
Finnegan et al. (2023)	Canada	Boreal forest	1–10 years	Field surveys (cover, seedling density)	Chronosequence with natural recovery thresholds
Bayramov et al. (2016)	Azerbaijan	Semi-arid steppe	5–10 years	Landsat/IKONOS NDVI + GIS	Multi-temporal remote sensing assessment
Ostermann et al. (2023)	Canada	Native rangeland	12 years	Field surveys (cover, composition)	Long-term monitoring with grazing treatments
Shaughnessy et al. (2021)	Canada	Boreal forest stockpiles	26–34 years	Field surveys (composition, richness)	Multi-decadal natural recovery assessment
Eduardo-Palomino et al. (2025)	Peru	Andean grasslands	9 years	Field surveys (species abundance, paired transects)	Yearly longitudinal monitoring with control comparisons

The absence of a statistically significant replanting effect ($p = 0.650$) reflects both methodological and temporal limitations. Limited sample size ($n = 3$ polygons) reduced statistical power, while Sentinel-2's 10 m resolution averaged localized vegetation gains across mixed planted and bare areas. The 95% CI (−0.064 to +0.103) encompasses modest positive effects typical of early restoration (Bright et al., 2019; Flemming et al., 2023). This indicates that the null result reflects a detection challenge rather than restoration inefficacy. The relatively short monitoring period post-intervention (27 months) may be insufficient to detect delayed establishment effects. The interrupted time-series specification assumes immediate detectability of intervention effects at the defined breakpoints. In the case of replanting, biological establishment and canopy development may involve delayed responses that are not immediately detectable at satellite resolution, particularly in Mediterranean climates.

A formal detectability analysis further clarifies this interpretation (Bloom, 1995; Bernal et al., 2017). Given the current design (n = 3 polygons), the minimum detectable site-wide level change at 80% power was ±0.119 NDVI and ± 0.079 NDRE. These thresholds exceed the observed replanting effects and are 1.7–4.0× larger than early-stage restoration signals commonly reported in forest systems (0.03–0.07 NDVI units). In contrast, the clearing disturbance substantially exceeded the detectability threshold, enabling robust detection. Together, these results confirm that the non-significant replanting effect reflects limited detectability at Sentinel-2 spatial resolution rather than a lack of vegetation establishment.

High-resolution UAV validation confirmed that localized vegetation establishment is occurring at fine spatial scales: UAV-derived NDVI and NDRE showed strong correlations with field-measured tree survival rates (r = 0.918 and 0.841, respectively). Each polygon contains only 10–17 Sentinel-2 pixels, and only a fraction of each polygon was replanted. This spatial scale mismatch is a well-documented challenge in moderate-resolution satellite monitoring of heterogeneous landscapes, where spectral responses represent unknown mixtures of vegetated and non-vegetated components (Vrieling et al., 2018; Malenovský et al., 2017; Dash et al., 2018; Daryaei et al., 2020). Field validation focused on early-stage restoration, where planted individuals were seedlings and saplings rather than mature trees. Structural metrics such as stem diameter were therefore not biologically meaningful at the time of survey. Correlation analyses were used descriptively to support interpretation rather than as primary inferential results, and Pearson correlation was applied for consistency with regression-based validation.

Natural recovery initiated during 2021–2022 may have further reduced the marginal contribution of replanting to overall greenness gains. This is consistent with Flemming et al. (2023), who showed that natural regeneration can offset early restoration effects where seed sources and soil seed banks persist. *Per*-polygon ITS estimates (Supplementary Table S3) revealed heterogeneity in natural recovery rates, with faster recovery in P1 (+0.126 NDVI yr^{-1}), moderate recovery in P3 (+0.064 yr^{-1}), and slower recovery in P2 (+0.031 yr^{-1}). However, replanting effects remained non-significant across all three polygons, suggesting that limited detectability reflects spatial resolution and sample size constraints rather than natural recovery masking effects in specific polygons. Climatic variability during the post-planting period likely moderated recovery potential. The distributed-lag analysis identified soil moisture as the dominant driver of vegetation variability, with positive effects at 0–1-month lags diminishing by 3 months, suggesting that short-term water deficits could have constrained early establishment. This interpretation is consistent with findings from Mediterranean and temperate ecosystems where water availability and energy supply are seasonally decoupled (Baldocchi et al., 2010; Jongen et al., 2011).

The apparent counterintuitive negative correlation between soil moisture and VIs in raw correlations (Fig. 7A and B) likely reflects the complex relationship between water availability and vegetation phenology in this system. High soil moisture often occurs during cooler periods with reduced photosynthetic activity, while moderate moisture stress during warmer periods can coincide with peak growing season vigor (Baldocchi et al., 2010; Jongen et al., 2011). In other words, months with higher evaporative demand tend to be followed by higher VI within 1–2 months, whereas moisture deficit relates to lower VI after a few months. Once seasonality is controlled for in the ITS framework, soil moisture's positive effect on vegetation becomes evident through the distributed-lag models. The climate-adjusted ITS framework effectively isolates anthropogenic intervention effects from seasonal and climatic confounding. Partial R^2 for the intervention block (Table 3) demonstrates that pipeline clearing and replanting explain substantial unique variance beyond seasonality, climate covariates, and polygon effects. This highlights the framework's ability to disentangle management interventions from background environmental variability. The climate-adjusted ITS framework requires known intervention dates and is best suited for abrupt, discrete disturbances. For unknown disturbance timing, breakpoint detection methods (e.g., BFAST; Verbesselt et al., 2010) can identify change dates, which can then be used as inputs to the ITS specification. For gradual changes, smooth functional forms could replace the immediate level-and-slope specification. The fixed-breakpoint approach represents a parsimonious proof-of-concept for known intervention timing.

Soil moisture emerged as the dominant climatic driver of NDVI and NDRE variability (Partial $R^2 = 0.19$–0.22), confirming that vegetation greenness in this system is primarily regulated by antecedent hydrological conditions rather than by instantaneous precipitation. This agrees with recent studies showing that vegetation integrates short-term cumulative water availability rather than discrete rainfall events (Ding et al., 2020; Walther et al., 2019; Vicente-Serrano et al., 2018). The relatively weak correlations with precipitation ($r \approx 0.16$–0.21) reinforce the value of including soil-moisture data in vegetation monitoring frameworks (Al-Kindi et al., 2023). The observed positive co-variation of evapotranspiration with NDVI and NDRE at short lags ($r \approx 0.33$–0.40) supports this seasonal coupling between evaporative demand and productivity. Neglecting lagged climatic influences can substantially bias estimates of disturbance and restoration effects (Lopez Bernal et al., 2018). Despite limited spatial replication, internal validity is strengthened by several design choices. Polygon fixed effects (δ_i) control for time-invariant differences among sites, including baseline vegetation, soil properties, and microsite conditions, isolating temporal intervention effects from static spatial heterogeneity. Month-clustered standard errors account for shared climatic shocks across polygons, providing conservative inference appropriate for the panel structure.

4.1. Limitations and future directions

Several methodological constraints affect interpretation and generalizability. The single-site design ($n = 3$ polygons, 0.42 ha) provides proof-of-concept but requires replication across diverse pipeline corridors and climatic contexts. This limitation is quantitatively demonstrated by the detectability analysis presented above. The relatively short post-replanting monitoring period (March 2023–May 2025, 27 months) may be insufficient to detect restoration benefits that emerge over longer timescales, particularly in temperate forest ecosystems where canopy closure can require 5–10 years. In addition, the ITS framework models replanting as an immediate level and trend change. However, seedling establishment and canopy development may involve delayed biological responses that only become spectrally detectable after several months to years. The use of ERA5-Land climate data (~9–11 km resolution) represents a necessary compromise when monitoring small, heterogeneous areas. Microclimatic heterogeneity related to slope, aspect, soil depth, or canopy structure may modulate vegetation responses to temperature and moisture, affecting climate VI relationships at fine spatial scales. In this study, ERA5-Land variables were included primarily to control for broad-scale temporal climate variability rather than to resolve within-site microclimatic gradients. Polygon fixed effects absorb time-invariant site characteristics such as slope, exposure, and soil properties, while the climate covariates capture regional month-to-month forcing shared across polygons. Any remaining microclimatic heterogeneity is therefore expected to increase residual variance rather than systematically bias intervention estimates, rendering inference conservative. Future applications may benefit from higher-resolution climate products or site-specific weather stations where available. Ground-based predictive models (height, biomass from VIs) were not attempted due to limited sampling ($n = 3$ polygons, single time point); such models require substantially larger and temporally replicated training datasets to avoid overfitting. Future applications monitoring small restoration projects should consider: (1) increasing polygon replication and size, (2) combining Sentinel-2 time-series with periodic UAV surveys to validate fine-scale heterogeneity, (3) implementing spatially replicated designs with paired treatment-control polygons where feasible, and (4) extending monitoring periods beyond 3–5 years to capture full restoration trajectories.

5. Conclusion

This proof-of-concept study demonstrates that climate-adjusted interrupted time-series analysis can robustly quantify vegetation disturbance and multi-year recovery at small spatial scales. Pipeline clearing caused immediate and substantial vegetation loss, followed by gradual natural recovery, while replanting in March 2023 showed no statistically detectable site-wide effect after accounting for climate and seasonality.

Multi-scale UAV validation confirmed that vegetation establishment was occurring at sub-pixel scales, highlighting the limitations of moderate-resolution satellite data for detecting early or spatially heterogeneous restoration signals. Taken together, these results underscore that the absence of a statistically significant replanting signal reflects detectability limits at moderate satellite resolution rather than a lack of ecological recovery. A formal detectability analysis further quantified these constraints, providing practical thresholds for future monitoring designs. By integrating Sentinel-2 and ERA5-Land observations, the proposed framework enables climate-aware attribution of vegetation change where traditional field-based controls are infeasible. Soil moisture emerged as the dominant short-lag climatic driver of vegetation variability, emphasizing the importance of hydrological conditions for post-disturbance recovery. The framework is broadly transferable to infrastructure-impacted landscapes, with the caveat that detecting subtle restoration effects requires larger sample sizes, longer monitoring periods, or higher-resolution imagery. From a management perspective, effective evaluation of restoration outcomes benefits from multi-year monitoring (≥3–5 years), attention to moisture constraints, and targeted high-resolution validation. Where seed sources persist, natural regeneration may provide a cost-effective pathway to recovery.

Supplementary data to this article can be found online at https://doi.org/10.1016/j.ecolind.2026.114670.

CRediT authorship contribution statement

Bojana Petrovic: Writing – original draft, Methodology, Investigation. **Mattia Balestra:** Writing – review & editing, Visualization, Conceptualization. **Tomáš Mikita:** Writing – review & editing. **Stefano Chiappini:** Data curation. **Roberto Pierdicca:** Supervision, Project administration, Funding acquisition.

Funding

The work was funded by Hystrix srl, within the joint research contract for the development of an innovative solution for monitoring, with remote and proximal sensing approaches, vegetation restoration after natural gas pipes installation.

Declaration of competing interest

The authors declare that they have no known competing financial interests or personal relationships that could have appeared to influence the work reported in this paper.

Acknowledgment

The authors acknowledge Hystrix srl for funding this research and for providing access to the study site.

Data availability

Data will be made available on request.

References

Abadie, A., Diamond, A., Hainmueller, J., 2010. Synthetic control methods for comparative case studies: estimating the effect of California's tobacco control program. J. Am. Stat. Assoc. 105 (490), 493–505. https://doi.org/10.1198/jasa.2009.ap08746.

Al-Kindi, K.M., Al Nadhairi, R., Al Akhzami, S., 2023. Dynamic change in normalised vegetation index (NDVI) from 2015 to 2021 in Dhofar, southern Oman in response to the climate change. Agriculture 13 (3), 592. https://doi.org/10.3390/agriculture13030592.

Angrist, J.D., Pischke, J.-S., 2009. Mostly harmless econometrics: an empiricist's companion. Princeton University Press. https://doi.org/10.2307/j.ctvcm4j72.

Asmala, E., Osburn, C.L., Paerl, R.W., Paerl, H.W., 2021. Elevated organic carbon pulses persist in estuarine environment after major storm events. Limnology and Oceanography Lett. 6 (1), 43–50. https://doi.org/10.1002/lol2.10169.

Balata, D., Gama, I., Domingos, T., Proença, V., 2022. Using satellite NDVI time-series to monitor grazing effects on vegetation productivity and phenology in heterogeneous Mediterranean forests. Remote Sens. 14 (10), 2322. https://doi.org/10.3390/rs14102322.

Balbuena, D., Alonso, A., Panta, M., Garcia, A., Gregory, T., 2019. Mitigating tropical forest fragmentation with natural and semi-artificial canopy bridges. Diversity 11 (4), 66. https://doi.org/10.3390/d11040066.

Baldocchi, D., Ma, S., Rambal, S., Misson, L., Ourcival, J.M., Limousin, J.M., Pereira, J., Papale, D., 2010. On the differential advantages of evergreenness and deciduousness in Mediterranean oak woodlands: A flux perspective. Ecol. Appl. 20 (6), 1583–1597. https://doi.org/10.1890/08-2047.1.

Barnes, E.M., Clarke, T.R., Colaizzi, P., Haberland, J., Kostrzewski, M., Riley, E., Moran, S., 2000. Coincident detection of crop water stress, nitrogen status, and canopy density using ground-based multispectral data. In proceedings of the fifth international conference on precision agriculture. July 16-19. Madison, WI: American Society of Agronomy.

Bayramov, E.R., Buchroithner, M.F., Bayramov, R.V., 2016. Multi-temporal assessment of ground cover restoration and soil erosion risks along petroleum and gas pipelines in Azerbaijan using GIS and remote sensing. Environ. Earth Sci. 75, 256. https://doi.org/10.1007/s12665-015-5044-9.

Beck, H.E., Zimmermann, N.E., McVicar, T.R., Vergopolan, N., Berg, A., Wood, E.F., 2018. Present and future Köppen-Geiger climate classification maps at 1-km resolution. Sci. Data 5, 180214. https://doi.org/10.1038/sdata.2018.214.

Bloom, H.S., 1995. Minimum detectable effects: A simple way to report the statistical power of experimental designs. Eval. Rev. 19 (5), 547–556. https://doi.org/10.1177/0193841X9501900504.

Brehm, T., Culman, S., 2022. Pipeline installation effects on soils and plants: a review and quantitative synthesis. Agrosystems, Geosciences & Environ. 5 (4), e20312. https://doi.org/10.1002/agg2.20312.

Bright, B.C., Hudak, A.T., Kennedy, R.E., Meddens, A.J.H., Evans, J.S., 2019. Examining post-fire vegetation recovery with Landsat time series analysis in the western United States. Fire Ecol. 15 (1), 8. https://doi.org/10.1186/s42408-018-0021-9.

Burkholder, J., Eggleston, D., Glasgow, H., Brownie, C., Reed, R., Janowitz, G., Posey, M., Melia, G., Kinder, C., Corbett, R., Toms, D., Alphin, T., Deamer, N., Springer, J., 2004. Comparative impacts of two major hurricane seasons on the Neuse River and western Pamlico Sound ecosystems. In: Proceedings of the National Academy of Sciences of the United States of America, 101, pp. 9291–9296. https://doi.org/10.1073/pnas.0306842101.

Cheng, Y., He, G., Luo, J., Gu, H., 2024. Effects of climate change on temperature sensitivity of vegetation growth in Huang-Huai-Hai plain: spatial-temporal dynamics and ecological adaptability. Remote Sens. 16 (21), 4024. https://doi.org/10.3390/rs16214024.

Conner, M.M., Saunders, W.C., Bouwes, N., et al., 2016. Evaluating impacts using a BACI design, ratios, and a Bayesian approach with a focus on restoration. Environ. Monit. Assess. 188, 555. https://doi.org/10.1007/s10661-016-5526-6.

Cohen, J., 1988. Statistical Power Analysis for the Behavioral Sciences, 2nd ed. Routledge. https://doi.org/10.4324/9780203771587.

Copernicus Climate Change Service, 2019. ERA5-land hourly data from 1950 to present [dataset]. Copernicus Climate Data Store (CDS). https://doi.org/10.24381/CDS.E2161BAC.

Dash, J.P., Pearse, G.D., Watt, M.S., 2018. UAV multispectral imagery can complement satellite data for monitoring forest health. Remote Sens. 10 (8), 1216. https://doi.org/10.3390/rs10081216.

Daryaei, A., Sohrabi, H., Atzberger, C., Immitzer, M., 2020. Fine-scale detection of vegetation in semi-arid mountainous areas with focus on riparian landscapes using Sentinel-2 and UAV data. Comput. Electron. Agric. 177, 105686. https://doi.org/10.1016/j.compag.2020.105686.

Del Río-Mena, T., Willemen, L., Vrieling, A., Nelson, A., 2023. How remote sensing choices influence ecosystem services monitoring and evaluation results of ecological restoration interventions. Ecosyst. Serv. 64, 101565. https://doi.org/10.1016/j.ecoser.2023.101565.

Delaporte, B., Ibanez, T., Despinoy, M., Mangeas, M., Menkes, C., 2022. Tropical cyclone impact and forest resilience in the southwestern Pacific. Remote Sens. 14 (5), 1245. https://doi.org/10.3390/rs14051245.

Delegido, J., Verrelst, J., Alonso, L., Moreno, J., 2011. Evaluation of Sentinel-2 red-edge bands for empirical estimation of green LAI and chlorophyll content. Sensors 11 (7), 7063–7081. https://doi.org/10.3390/s110707063.

Delloye, C., Weiss, M., Defourny, P., 2018. Retrieval of the canopy chlorophyll content from Sentinel-2 spectral bands to estimate nitrogen uptake in intensive winter wheat cropping systems. Remote Sens. Environ. 216, 245–261. https://doi.org/10.1016/j.rse.2018.06.037.

Ding, Y., Li, Z., Peng, S., 2020. Global analysis of time-lag and accumulation effects of climate on vegetation growth. Int. J. Appl. Earth Observation and Geoinformation 92, 102179. https://doi.org/10.1016/j.jag.2020.102179.

Dronova, I., Taddeo, S., 2022. Remote sensing of phenology: towards comprehensive indicators of plant community dynamics from species to regional scales. J. Ecol. 110 (7), 1460–1484. https://doi.org/10.1111/1365-2745.13897.

Drusch, M., Del Bello, U., Carlier, S., Colin, O., Fernandez, V., Gascon, F., Hoersch, B., Isola, C., Laberinti, P., Martimort, P., Meygret, A., Spoto, F., Sy, O., Marchese, F., Bargellini, P., 2012. Sentinel-2: ESA'S optical high-resolution mission for GMES operational services. Remote Sens. Environ. 120, 25–36. https://doi.org/10.1016/j.rse.2011.11.026.

Eduardo-Palomino, F., Chuquillanqui, H., Linares-Palomino, R., 2025. Unveiling vegetation recovery dynamics in Andean grasslands along a trans-Andean natural gas pipeline. Ecol. Indic. 170, 112884. https://doi.org/10.1016/j.ecolind.2024.112884.

England, J., Angelopoulos, N., Cooksley, S., Dodd, J., Gill, A., Gilvear, D., Johnson, M., Naura, M., O'hare, M., Tree, A., Wheeldon, J., Wilkes, M.A., 2021. Best practices for monitoring and assessing the ecological response to river restoration. Water 13 (23), 3352. https://doi.org/10.3390/w13233352.

Filicetti, A.T., Nielsen, S.E., 2020. Tree regeneration on industrial linear disturbances in treed peatlands is hastened by wildfire and delayed by loss of microtopography. Can. J. For. Res. 50 (9), 936–945. https://doi.org/10.1139/cjfr-2019-0451.

Finnegan, L., Hebblewhite, M., Pigeon, K.E., 2023. Whose line is it anyway? Moose (Alces alces) response to linear features. Ecosphere 14, e4636. https://doi.org/10.1002/ecs2.4636.

Flemming, B.H., Futoransky, V., Pruett, W., 2023. Quantifying restoration success via natural recovery in forested areas following pipeline construction. Restoration Ecology 31 (3), e13749. https://doi.org/10.1111/rec.13749.

Galdelli, A., Pesaresi, S., Quattrini, G., Pierdicca, R., Thaliath, A.B., Mancini, A., 2025. VegRecoverAI: a deep learning-based system for automated vegetation recovery assessment and prediction with demonstration case study on gas pipeline construction. Environ. Model. Software 193, 106601. https://doi.org/10.1016/j.envsoft.2025.106601.

Gao, B.C., 1996. NDWI-A normalized difference water index for remote sensing of vegetation liquid water from space. Remote Sens. Environ. 58 (3), 257–266. https://doi.org/10.1016/S0034-4257(96)00067-3.

Gao, X., Gray, A., Reich, P.B., 2024. Humid, warm and treed ecosystems show longer time-lag of vegetation response to climate. Geophys. Res. Lett. 51 (18), e2024GL111737. https://doi.org/10.1029/2024GL111737.

Gitelson, A.A., Kaufman, Y.J., Merzlyak, M.N., 1996. Use of a green channel in remote sensing of global vegetation from EOS-MODIS. Remote Sens. Environ. 58 (3), 289–298. https://doi.org/10.1016/S0034-4257(96)00072-7.

Gitelson, A.A., Viña, A., Arkebauer, T.J., Rundquist, D.C., Keydan, G., Leavitt, B., 2003. Remote estimation of leaf area index and green leaf biomass in maize canopies. Geophys. Res. Lett. 30 (5), 1248. https://doi.org/10.1029/2002GL016450.

Gorelick, N., Hancher, M., Dixon, M., Ilyushchenko, S., Thau, D., Moore, R., 2017. Google earth engine: planetary-scale geospatial analysis for everyone. Remote Sens. Environ. 202, 18–27. https://doi.org/10.1016/j.rse.2017.06.031.

Huete, A.R., 1988. A soil-adjusted vegetation index (SAVI). Remote Sens. Environ. 25 (3), 295–309. https://doi.org/10.1016/0034-4257(88)90106-X.

Jongen, M., Pereira, J.S., Aires, L.M.I., Pio, C.A., 2011. The effects of drought and timing of precipitation on the inter-annual variation in ecosystem-atmosphere exchange in a Mediterranean grassland. Agric. For. Meteorol. 151 (5), 595–606. https://doi.org/10.1016/j.agrformet.2011.01.008.

Kang, Y., Wang, Z., Xu, B., Shen, W., Chen, Y., Zhou, X., Liu, Y., Zhang, T., Wang, G., Jia, Y., Li, J., 2024. Disentangling the response of vegetation dynamics to natural and anthropogenic drivers over the Minjiang River basin using dimensionality reduction and a structural equation model. Forests 15 (8), 1438. https://doi.org/10.3390/f15081438.

Kennedy, R.E., Yang, Z., Cohen, W.B., 2010. Detecting trends in forest disturbance and recovery using yearly Landsat time series: 1. LandTrendr-temporal segmentation algorithms. Remote Sens. Environ. 114 (12), 2897–2910. https://doi.org/10.1016/j.rse.2010.07.008.

Lasaponara, R., Abate, N., Fattore, C., Aromando, A., Cardettini, G., Di Fonzo, M., 2022. On the use of Sentinel-2 NDVI time series and Google earth engine to detect land-use/land-cover changes in fire-affected areas. Remote Sens. 14 (19), 4723. https://doi.org/10.3390/rs14194723.

Linden, A., 2015. Conducting interrupted time-series analysis for single- and multiple-group comparisons. Stata J. 15 (2), 480–500. https://doi.org/10.1177/1536867X1501500208.

Lopez Bernal, J., Cummins, S., Gasparrini, A., 2017. Interrupted time series regression for the evaluation of public health interventions: A tutorial. Int. J. Epidemiol. 46 (1), 348–355. https://doi.org/10.1093/ije/dyw098.

Lopez Bernal, J., Soumerai, S., Gasparrini, A., 2018. A methodological framework for model selection in interrupted time series studies. J. Clin. Epidemiol. 103, 82–91. https://doi.org/10.1016/j.jclinepi.2018.05.026.

MacDonald, A., Bartels, S.F., Macdonald, S.E., Pigeon, K.E., MacNearney, D., Finnegan, L., 2020. Wildlife forage cover and composition on pipeline corridors in Alberta: implications for wildlife conservation. For. Ecol. Manage. 468, 118189. https://doi.org/10.1016/j.foreco.2020.118189.

Malenovský, Z., Lucieer, A., King, D.H., Turnbull, J.D., Robinson, S.A., 2017. Unmanned aircraft system advances health mapping of fragile polar vegetation. Methods Ecol. Evol. 8 (12), 1842–1857. https://doi.org/10.1111/2041-210X.12833.

McFeeters, S.K., 1996. The use of the normalized difference water index (NDWI) in the delineation of open water features. Int. J. Remote Sensing 17 (7), 1425–1432. https://doi.org/10.1080/01431169608948714.

Mehmood, K., Anees, S.A., Muhammad, S., Hussain, K., Shahzad, F., Liu, Q., Ansari, M.J., Alharbi, S.A., Khan, W.R., 2024. Analyzing vegetation health dynamics across seasons and regions through NDVI and climatic variables. Sci. Rep. 14, 11775. https://doi.org/10.1038/s41598-024-62464-7.

Meroni, M., Schucknecht, A., Fasbender, D., Rembold, F., Fava, F., Mauclaire, M., Goffner, D., Di Lucchio, L.M., Leonardi, U., 2017. Remote sensing monitoring of land restoration interventions in semi-arid environments with a before-after control-impact statistical design. Int. J. Appl. Earth Observation and Geoinformation 59, 42–52. https://doi.org/10.1016/j.jag.2017.02.016.

Monroe, A.P., Aldridge, C.L., O'Donnell, M.S., Manier, D.J., Homer, C.G., Anderson, P.J., 2020. Using remote sensing products to predict recovery of vegetation across space and time following energy development. Ecol. Indic. 110, 105872. https://doi.org/10.1016/j.ecolind.2019.105872.

Muñoz-Sabater, J., et al., 2021. ERA5-land: a state-of-the-art global reanalysis dataset for land applications. Earth System Science Data 13 (9), 4349–4383. https://doi.org/10.5194/essd-13-4349-2021.

Naeth, M.A., Locky, D.A., Wilkinson, S.R., 2020. Pipeline impacts and recovery of dry mixed-grass prairie soil and plant communities. Rangel. Ecol. Manage. 73 (5), 619–628. https://doi.org/10.1016/j.rama.2020.06.003.

Ostermann, D.K., Dhar, A., Naeth, M.A., 2023. Native and dryland pasture seed mixes impact revegetation 12 years after pipeline construction in southern Alberta. Land 12 (4), 921. https://doi.org/10.3390/land12040921.

Pałaś, K.W., Zawadzki, J., 2020. Sentinel-2 imagery processing for tree logging observations on the Białowieża Forest world heritage site. Forests 11 (8), 857. https://doi.org/10.3390/f11080857.

Pickell, P.D., Hermosilla, T., Frazier, R.J., Coops, N.C., Wulder, M.A., 2016. Forest recovery trends derived from Landsat time series for north American boreal forests. Int. J. Remote Sens. 37 (1), 138–149. https://doi.org/10.1080/2150704X.2015.1126375.

Peel, M.C., Finlayson, B.L., McMahon, T.A., 2007. Updated world map of the Köppen-Geiger climate classification. Hydrol. Earth Syst. Sci. 11 (5), 1633–1644. https://doi.org/10.5194/hess-11-1633-2007.

Qi, J., Chehbouni, A., Huete, A.R., Kerr, Y.H., Sorooshian, S., 1994. A modified soil adjusted vegetation index. Remote Sens. Environ. 48 (2), 119–126. https://doi.org/10.1016/0034-4257(94)90134-1.

Raiter, K.G., Prober, S.M., Possingham, H.P., Westcott, F., Hobbs, R.J., 2018. Linear infrastructure impacts on landscape hydrology. J. Environ. Manage. 206, 446–457. https://doi.org/10.1016/j.jenvman.2017.10.036.

Ramsay, C.R., Matowe, L., Grilli, R., Grimshaw, J.M., Thomas, R.E., 2003. Interrupted time series designs in health technology assessment: lessons from two systematic reviews of behavior change strategies. Int. J. Technol. Assess. Health Care 19 (4), 613–623. https://doi.org/10.1017/S0266462303000576.

Shaughnessy, B.E., Dhar, A., Naeth, M.A., 2021. Natural recovery of vegetation on reclamation stockpiles after 26 to 34 years. Écoscience 29 (1), 55–67. https://doi.org/10.1080/11956860.2021.1943931.

Shi, P., Xiao, J., Wang, Y.-F., Chen, L.-D., 2014. The effects of pipeline construction disturbance on soil properties and restoration cycle. Environ. Monit. Assess. 186 (3), 1825–1835. https://doi.org/10.1007/s10661-013-3496-5.

Smokorowski, K.E., Randall, R.G., 2017. Cautions on using the before-after-control-impact design in environmental effects monitoring programs. FACETS 2 (1), 212–232. https://doi.org/10.1139/facets-2016-0058.

Taddeo, S., Dronova, I., Depsky, N., 2022. Leveraging time series of satellite and aerial images to promote the long-term monitoring of restored plant communities. Appl. Veg. Sci. 25 (2), e12664. https://doi.org/10.1111/avsc.12664.

Tucker, C.J., 1979. Red and photographic infrared linear combinations for monitoring vegetation. Remote Sens. Environ. 8 (2), 127–150. https://doi.org/10.1016/0034-4257(79)90013-0.

Verbesselt, J., Hyndman, R., Newnham, G., Culvenor, D., 2010. Detecting trend and seasonal changes in satellite image time series. Remote Sens. Environ. 114 (1), 106–115. https://doi.org/10.1016/j.rse.2009.08.014.

Vicente-Serrano, S.M., Gouveia, C., Camarero, J.J., Beguería, S., Trigo, R., López-Moreno, J.I., Azorín-Molina, C., Pasho, E., Lorenzo-Lacruz, J., Revuelto, J., Morán-Vrieling, A., Meroni, M., Darvishzadeh, R., Skidmore, A.K., Wang, T., Zurita-Milla, R., Toxopeus, A.G., 2018. Vegetation phenology from Sentinel-2 and field cameras for a Dutch barrier island. Remote Sensing of Environ. 215, 517–529. https://doi.org/10.1016/j.rse.2018.03.014.

Wagner, A.K., Soumerai, S.B., Zhang, F., Ross-Degnan, D., 2002. Segmented regression analysis of interrupted time series studies in medication use research. J. Clin. Pharm. Ther. 27 (4), 299–309. https://doi.org/10.1046/j.1365-2710.2002.00430.x.

Walther, S., Duveiller, G., Jung, M., Guanter, L., Cescatti, A., Reichstein, M., 2019. Satellite observations of the contrasting response of trees and grasses to variations in water availability. Geophysical Research Letters 46 (7), 4039–4049. https://doi.org/10.1029/2018GL080535.

Wauchope, H.S., Amano, T., Geldmann, J., Johnston, A., Simmons, B.I., Sutherland, W.J., Jones, J.P.G., 2021. Evaluating impact using time-series data. Trends in Ecology & Evolution 36 (3), 196–205. https://doi.org/10.1016/j.tree.2020.11.001.

White, J.C., Wulder, M.A., Hermosilla, T., Coops, N.C., Hobart, G.W., 2017. A nationwide annual characterization of 25 years of forest disturbance and recovery for Canada using Landsat time series. Remote Sensing of Environ. 194, 303–321. https://doi.org/10.1016/j.rse.2017.03.035.

Wortley, L., Hero, J.M., Howes, M., 2013. Evaluating ecological restoration success: a review of the literature. Restoration Ecol. 21 (5), 537–543. https://doi.org/10.1111/rec.12028.

WWF & Center for Large Landscape Conservation, 2025. Incorporating Natural Resource Safeguards in Linear Infrastructure Planning: A Compendium of Best Practice Resources. WWF, Washington, DC.

Xiao, J., Shi, P., Wang, Y., Yang, L., 2016. The vegetation recovery pattern and affecting factors after pipeline disturbance in northwest China. J. Nat. Conservation 29, 114–122. https://doi.org/10.1016/j.jnc.2015.12.009.

Xiao, J., Wang, Y., Shi, P., Yang, L., Chen, L., 2014. Potential effects of large linear pipeline construction on soil and vegetation in ecologically fragile regions. Environ. Monitoring and Assessment 8037–8048. https://doi.org/10.1007/s10661-014-3986-0.

Yan, K., Gao, S., Yan, G., Ma, X., Chen, X., Zhu, P., Li, J., Gao, S., Gastellu-Etchegorry, J.-P., Myneni, R.B., Wang, Q., 2025. A global systematic review of the remote sensing vegetation indices. Int. J. Appl. Earth Observation and Geoinformation 139, 104560. https://doi.org/10.1016/j.jag.2025.104560.

Zhao, F., Huang, C., Goward, S.N., Schleeweis, K., Rishmawi, K., Lindsey, M.A., Denning, E., Keddell, L., Cohen, W.B., Yang, Z., Dungan, J.L., Michaelis, A., 2018. Development of Landsat-based annual U.S. forest disturbance history maps (1986-2010) in support of the North American Carbon Program (NACP). Remote Sensing of Environ. 209, 312–326. https://doi.org/10.1016/j.rse.2018.02.035.

Zhu, Z., Woodcock, C.E., 2014. Continuous change detection and classification of land cover using all available Landsat data. Remote Sensing of Environ. 144, 152–171. https://doi.org/10.1016/j.rse.2014.01.011.

Zhu, Z., Zhang, J., Yang, Z., Aljaddani, A.H., Cohen, W.B., Qiu, S., Zhou, C., 2020. Continuous monitoring of land disturbance based on Landsat time series. Remote Sensing of Environ. 238, 111116. https://doi.org/10.1016/j.rse.2019.03.009.